PPPL-3309, Preprint: July 1998, UC-420

Global Confinement, Sawtooth Mixing and Stochastic Diffusion Ripple Loss of Fast ICRF-Driven H^+ Minority Ions in TFTR

M. P. Petrov*, R. Bell, R. V. Budny, N. N. Gorelenkov**, S. S. Medley and S. J. Zweben.

Princeton Plasma Physics Laboratory, P. 0. Box 451, Princeton, NJ, 08543, USA
** A. F. Ioffe Physical-Technical Institute, St. Petersburg, 194021, Russia*
*** TRINITI, Troitsk, 142092, Russia.*

Abstract

This paper presents studies of ICRF-driven H^+ minority ions in TFTR deuterium plasmas using primarily passive H^o flux detection in the energy range of 0.2 - 1.0 MeV with some corroborating active (Li pellet charge exchange) measurements. It is shown that in the passive mode the main donors for the neutralization of H^+ ions in this energy range are C^{5+} ions. The measured effective H^+ tail temperatures range from 0.15 MeV at an ICRF power of 2 MW to 0.35 MeV at 6 MW. Analysis of the ICRF-driven H^+ ion energy balance has been performed on the basis of the dependence of effective H^+ temperatures on the plasma parameters. The analysis showed that H^+ confinement times are comparable with their slowing down times and tended to decrease with increasing ICRF power.

Radial redistribution of ICRF-driven H^+ ions was detected when giant sawtooth crashes occurred during the ICRF heating. The redistribution affected ions with energy below 0.7-0.8 MeV. The sawtooth crashes displace H^+ ions outward along the plasma major radius into the stochastic ripple diffusion domain were those ions are lost in ~ 10 milliseconds. These observations are consistent with the model of the redistribution of energetic particles developed previously to explain the results of DT alpha particle redistribution due to sawteeth observed in TFTR. The experimental data are also consistent with ORBIT code simulations of H^+ stochastic ripple diffusion losses.

I. Introduction

Studies of the ICRF-driven H^+ minority in deuterium TFTR plasmas were performed using neutral particle analysis in the energy range of 0.2 - 1 MeV. The neutral particle measurements were obtained using a high energy neutral particle analyzer (NPA) developed by the Ioffe Institute [1]. Similar measurements were performed earlier on JET where the efficient passive neutralization of MeV energy protons was first observed in the plasma core [2,3]. The main donors for the neutralization of the protons appeared be the hydrogen-like low Z impurity ions. In a later paper [4], a detailed analysis of the neutralization processes of MeV protons in JET was made and the cross sections of the electron capture by H^+ ions from C^{5+} and Be^{3+} ions (the main donors in JET plasmas) were calculated. Similar measurements of the ICRF-driven H^+ minority have also been made on JT-60U [5].

The high energy NPA was used on TFTR primarily for Pellet Charge Exchange (PCX) diagnostics [6,7] wherein active charge exchange measurements of the energy and radial distributions of DT alpha particles were obtained in conjunction with impurity pellet injection and the detector operated in the current mode. In parallel, passive measurements of H^+ ICRF-driven minority ions at energies up to the MeV range were also performed in the pulse counting mode provided the count rate remained relatively low (~ 10 kHz). In the last stage of the TFTR experiments, the pulse counting capability was upgraded by implementing a detector system developed at the Ioffe Institute and previously operated on JET and JT-60U [5] which extended the count rate capability up to ~ 1 MHz. This system consisted of Cs(Tl) scintillators designed to minimize the signals produced by background neutrons and gamma rays and was equipped with 16-channel pulse height electronics (ADC) on each of the eight NPA energy channels. Fig. 1 shows the number of H^+ counts detected by the ADC in the third NPA energy channel (E_{H^+} = 0.3 MeV) during a period of 200 ms. H^+ counts appear in ADC channels 5 - 14 (shaded area) with the maximum in channel 11. The low amplitude pulses in channels 1 - 4 are the n,γ background and the detector noise. It is seen that the noise and background are easily distinguished from the H^+ signal which made it reasonable to use this system in the presence of high n,γ background. In the absence of significant background when higher time resolution was desired (as in the case of H^+ sawtooth mixing studies in TFTR during D plasma operation with ICRF-driven H^+ minority heating), the current mode was used but with the discrimination threshold reduced and an integration time of 1 - 10 μs.

The experimental data presented in this paper are mainly the results of operation in the passive pulse counting mode.

II. Physical Basis of the Passive Charge Exchange Diagnostic

As was mentioned above, passive measurement of the ICRF-driven H^+ minority ions in the MeV energy range is based on electron capture by H^+ ions from hydrogen-like low-Z impurity ions. The most probable donors for electron capture in TFTR plasmas are C^{5+} ions because the main low-Z impurity was carbon. In principle, another possible donor could be the residual D^o atoms. The cross sections for charge exchange of H^+ with D^o atoms [8] and C^{5+} impurity ions [4] are shown in Fig. 2. The charge-exchange rates of H^+ on D^o and C^{5+} are shown in Fig. 3. Here the density of C^{5+} in the plasma core is equal to 10^{10} cm^{-3} (estimated on the basis of spectroscopic measurements) and the upper limit of D^o density is estimated to be ~10^8 cm^{-3}. The energy range of the NPA measurements is also indicated. It is clearly seen from the figure that the dominant donor in TFTR plasmas in the energy range of the interest is C^{5+}. Therefore, we can conclude that the NPA detects the H^o passive signal as a result of the reaction:

$$H^+ + C^{5+} = H^o + C^{6+}. \qquad (1)$$

In this case the H^o flux produced in the plasma can be expressed as:

$$\Phi_{Ho}(E) = n_{H^+} n_{C^{5+}} f_{H^+}(E) \sigma v_{H^+} \quad (cm^3\ s\ eV)^{-1} \qquad (2)$$

where n_{H^+}, $n_{C^{5+}}$ are the densities of H^+ and C^{5+} ions in the plasma, $f_{H+}(E)$ is the local H^+ energy distribution function, σ is the cross section of the reaction shown in Eq. (1), and v_{H+} is the H^+ velocity.

The NPA was located in the midplane and had an observation line at a toroidal angle equal to 2.75^o to the major radius direction. Therefore only deeply trapped ions with pitch angles in a narrow range $v_{||}/v = -0.048 \pm 10^{-3}$ were detected. The measured energy spectrum integrated over the observation sightline, L, can be expressed as:

$$dn_{Ho}/dE = \int_L \Phi_{Ho}(E,l) \exp\{-\int_L N_e(x)\, \sigma_r(E)\, dx\}\, dl \qquad (3)$$

where $N_e(x)$ is the electron density and $\sigma_r(E)$ is the sum of the cross sections for reionization of fast H^o atoms emerging from the plasma due to collisions with electrons and deuterons including charge exchange reactions. Here exp{..} represents the transparency, $\mu(E)$, of the plasma for the detected H^o atoms. This transparency is not a significant factor

for the sub MeV and MeV H^o atoms in TFTR and has to be taken into account only for the low energy part of the NPA energy range shown in Fig. 2 and Fig. 3.

The energy spectrum of H^+ ions can be derived from the number of counts in the n^{th} channel of the NPA, $N_n(E)$, in the following way:

$$dn_{H^+}/dE \sim N_n(E) \{\sigma v_{H^+} \eta (E) \Delta E_n\}^{-1}. \quad (4)$$

Here η (E) is the calibrated NPA detection efficiency and ΔE_n is the energy width of the n^{th} channel. In the case of the ICRF-driven ions in TFTR, this yields $dn_{H^+}/dE \sim f_{H^+}(E)$ averaged over the ICRF resonance layer because the $n_{H^+} n_{C^{5+}}$ product is sensibly constant when the ICRF resonance is located in the plasma core, as illustrated by the schematic shown in Fig. 4.

Active PCX measurements obtained with the use of the Li pellets injected into the plasma [9] were also used in some cases for measuring the H^+ tail distributions. In this case, H^+ ICRF-driven ions interacted with the pellet ablation cloud and formed an equilibrium neutral fraction, F_o (E), as a result of the reaction:

$$H^+ + Li^+ => H^o + Li^{2+}. \quad (5)$$

The energy distribution derived from PCX active signals can be expressed as:

$$dn_{H^+}/dE \sim \Gamma_n(E_n)\{F_o(E) v_{H^+} \eta(E) \Delta E_n\}^{-1} \quad (6)$$

where $\Gamma_n(E_n)$ is the measured PCX signal in the n^{th} channel of the NPA in the current mode with units of volts.

Figure 5 presents the active PCX signal versus pellet flight time for the NPA channel which detected H^+ ions of energy 0.72 MeV. This signal was taken during the ICRF fundamental on-axis heating of H^+ minority in a deuterium plasma (#96085, ICRF frequency 43 MHz, TF coil current 45 kA, ICRF power 2.1 MW). On the horizontal axis, the radial position of the pellet is shown as derived from the measured pellet velocity (653 ms^{-1}). The contour of the signal measured by the PCX diagnostic corresponds to the radial position, shape and width (ΔR = 6.1 cm) of the H^+ resonance. The low level passive signal is also seen before and after the pellet signal.

Figure 6 shows the active energy spectrum of ICRF-driven H^+ ions for the discharge presented in Fig. 5 and the passive spectrum averaged over 100 ms during an ICRF power pulse in a discharge with the same parameters (#96080). It is seen that active

and passive spectra have the same Maxwellian shapes and very similar effective tail temperatures. This provides additional evidence that the proper donor (C^{5+}) was chosen to derive the passive energy spectrum.

III. Global ICRF-Driven H^+ Minority Ion Confinement

The passive measurements of H^+ ICRF-driven minority ion temperature in deuterium plasmas were performed routinely mainly as "piggy-back" experiments during ICRF runs on the TFTR. Figure 7 presents the effective temperature, $T(H^+)$, of the H^+ minority versus ICRF power, P_{ICRF}, for a collection of 67 discharges. The measurements were made in deuterium on-axis, ICRF-heated discharges for the following range of plasma parameters: I_{plasma} = (1.3 - 1.8) MA, $N_e(0) = (2.4 - 6.0)10^{13}$ cm^{-3} and $T_e(0)$ = (2.6-10) keV. It can be seen that $T(H^+)$ increased monotonically with P_{ICRF} but even for P_{ICRF} ~ 6 MW, the values of $T(H^+)$ do not exceed ~ 0.35 MeV. In an attempt explain these relatively low values of $T(H^+)$, we constructed a scaling of $T(H^+)$ versus plasma parameters on the basis of the global energy balance for the H^+ minority which includes the ICRF heating and assumes limited H^+ confinement in terms of the quasi-neoclassical diffusion [10].

The ICRF-heated H^+ energy balance can be described by the following equation:

$$1.5\, N_e\, T(H^+)/\tau_c + 1.5\, N_e\, T(H^+)/\tau_{slow} = P_{ICRF}/\alpha. \qquad (7)$$

We assume that $N(H^+) = \alpha N_e$, where $N(H^+)$ is the density of H^+ minority ions, N_e is the electron density, and $N(H^+)/N_e = \alpha$ is a constant for all shots included in the analysis. Typically α = 0.05 - 0.1 << 1. In the Eq. (1), τ_c, and τ_{slow} are the confinement and slowing down times, respectively, of the ICRF-driven H^+ ions.

To simulate the confinement time, τ_c, we assumed a neoclassical type diffusion with characteristic displacement step equal to the banana width, $\Delta = qr_L/\varepsilon^{1/2}$, where r_L is the Larmor radius and ε is the inverse aspect ratio. With this approach one can obtain $\tau_c = a^2/D$ where the diffusion rate, $D \equiv \Delta^2/\tau_D$, can be written as $D = (r_L q)^2/\varepsilon\tau_D$ with τ_D being the characteristic diffusion time. The confinement time can be expressed in the following way:

$$\tau_c = \tau_D\, I_{pl}^2\, /[T(H^+)\varepsilon]$$

or

$$\tau_c = C_c\, I_{pl}^2/T(H^+), \qquad (8)$$

where I_{pl} is the plasma current (MA), $T(H^+)$ is the H^+ effective temperature (MeV) and C_C is a dimensional constant proportional to the diffusion time, τ_D. Then we can use the expression for slowing down time,

$$\tau_{slow}(sec) = 0.1 T_e(keV)^{3/2}/N_e\ (10^{13} cm^{-3}) \qquad (9)$$

and write

$$\tau_c = \tau_{slow} 10\ C_C\ [I_{pl}^2\ N_e\ /T_e^{3/2} T(H^+)]. \qquad (10)$$

Substituting Eqs. (9) and (10) (where all variables have the dimensions as indicated above) into the energy balance, Eq. (7) yields a quadratic equation for $T(H^+)$ whose solution is:

$$T(H^+) = (0.01 C_C^2 A^2 + P_{ICRF} I_{pl}^2\ 1.5\ C_C/N_e\alpha)^{1/2} - 0.1 C_C A = F(C_C,\alpha) \qquad (11)$$

where $A = N_e I_{pl}^2/2T_e^{3/2}$.

Our aim is to define the value C_C using the dependence $T(H^+) = F(C_C,\alpha)$. By arranging for the plot of $T(H^+) = F(C_C,\alpha)$ to go through zero by varying C_C as a free parameter assuming $\alpha = 0.05$, we obtain $C_C = 0.018 \pm 0.001$. The corresponding scaling is shown in Fig. 8. It can be shown that increasing α from 0.5 to 0.1 leads to a 20% decrease of C_C.

Knowing the value of C_C, we can estimate the ratio τ_c/τ_{slow} and the absolute value of τ_c. Figures 9 and 10 present these values versus P_{ICRF}. The figures show that the ratio τ_c/τ_{slow} for H^+ ICRF-driven ions in TFTR is close to unity and deteriorates slowly with the increasing ICRF power. The confinement time, τ_c, also deteriorates with increasing ICRF power from ~ 0.3 s at 0.8 MW to ~ 0.18 s at 6 MW. This means that significant losses of H^+ ICRF-driven ions exist in TFTR which increase with increasing ICRF power. The reason for this could be the existence of MHD activity (TAE-like modes) described in the paper [11]. This paper indicated that increasing the ICRF power above ~ 3 MW and generation of an ICRF-driven H^+ high energy tail leads to a sharp increase of the TAE mode amplitude detected by Mirnov coils at the plasma edge in the range of 150 - 200 kHz. The presence of TAE modes can lead to fast ion redistribution inside the plasma and to the diffusion-like losses of fast H^+ ions which we described above.

IV. Sawtooth Mixing of ICRF-Driven Fast H^+ Ions

a) Experimental Observations

The effective temperatures, $T(H^+)$, presented above were measured in quiescent plasma in the absence of strong low frequency MHD events like giant sawtooth crashes or disruptions. Now we will describe the behavior of ICRF-driven H^+ minority ions in the presence of strong MHD events like a giant sawtooth crash in TFTR.

The influence of sawtooth oscillations on fast ions in tokamaks is of considerable interest because theoretical studies showed they can lead to a significant redistribution of the ions [12]. The influence of sawtooth effects on injected neutral beam ions and fusion products in DD plasmas has been discussed elsewhere [13, 14]. During DT experiment on TFTR, the PCX diagnostic revealed strong transport of trapped MeV alpha particles radially outward well beyond q=1 surface after sawtooth crashes [15 - 17].

Figure 11 presents the signal for H^+ ions (0.266 MeV) and x-rays showing two giant sawtooth crashes, the signal of lost H^+ ions measured by the lost alpha detector [18] located 60^o below the outer midplane on the wall of the vacuum vessel and the signal indicating TAE modes in the range of 150 - 200 kHz measured with the Mirnov coils. We see here that at the time of giant sawtooth crashes, a dramatic increase of the 0.266 MeV H^+ signal occurs and also sharp spikes on the H^+ lost ions. We note that the lost ion signal is averaged over the pitch angle range 45^o - 83^o and an H^+ energy range 0.4 - 2 MeV. It is interesting that rather strong TAE activity does not appear to directly affect the measured H^+ signal of the deeply trapped ions.

Figure 12 presents the H^+ signal taken from the 1st, 3rd and 7th channels of the NPA detecting H^+ at energies of 0.266 MeV, 0.404 MeV and 0.855 MeV. It is seen that the influence of the crashes on the signal diminishes with increasing of H^+ energy and completely disappears at an H^+ energy of 0.855 MeV. The time decay of the spikes in the 1st and 3rd channels is a few milliseconds.

The schematic presented in Fig. 13 illustrates the qualitative model which we propose to explain detected H^+ spikes in the presence of sawtooth crashes and their subsequent time decay . The H^+ resonance layer shown here is located near the plasma center. Immediately after the crash, H^+ ions can be redistributed and moved outwards (the H^+ mixing radius, r_{mix}, is shown). The C^{5+} radial density profile has the shape shown in the Fig. 13 (the C^{5+} density increases near the plasma periphery). If r_{mix} is large enough to reach the region with increasing C^{5+} density, a sharp increase of H^+ signal will occur. The stochastic ripple diffusion domain is located in the outer region of the tokamak plasma

where fast H^+ ions will be lost in a few milliseconds [19]. The expected position of the stochastic domain for sub-MeV H^+ ions is shown on the schematic. The poor confinement of the H^+ ions displaced by the sawtooth crash into the stochastic domain leads to the detected decay of the signal. This scenario is also consistent with the signals for lost H^+ ions. It is seen that the time decay of the lost ion signal is very close to that of the H^+ passive charge exchange signal. Outward of the stochastic domain there is the region of prompt losses. Losses of this kind are also seen on the lost H^+ signal. We see here very sharp spikes (prompt losses) and delayed losses corresponding to the stochastic ripple diffusion. Below this model will be presented quantitatively.

b) Modeling of ICRF-Driven H^+ Sawtooth Mixing in TFTR.

We have mentioned above that during DT experiments on TFTR the redistribution of alpha particles due to sawtooth crashes was observed. To explain this redistribution a model of alpha sawtooth mixing was developed [20] based on the fast particle orbit averaged toroidal drift in a perturbed helical electric field generated by the sawtooth crash with an adjustable absolute value. Such a drift of fast particles results in a change of their energy and a redistribution in phase space. This model agreed well the measured alpha particle redistribution due to sawtooth mixing [16, 17].

In this paper, the model is applied to ICRF-driven H^+ ions to describe the experimentally measured H^+ redistribution presented above. The results of the H^+ redistribution modeling are shown in Fig. 14. Here we see the ICRF H^+ precrash resonance contours for the energies 0.25 MeV, 0.5 MeV and 0.75 MeV located in the TFTR plasma core. An initial precrash distribution function was chosen as Maxwellian in energy with effective temperature $T(H^+)$ = 269 keV (in accordance with the measurements) and Gaussian in pitch angle, so that H^+ ions are localized near the ICRH resonance layer. The resonance location is taken from the frequency and toroidal field values. The width of the resonance is taken to be 10 cm. Plasma equilibrium and other parameters were taken from TRANSP Monte Carlo code [21].

The model predictions of the redistribution after the crash are also shown in Fig. 14. The mixing radius used for modeling was determined from the Kadomtsev reconnection model [22] on the basis of q profiles from TRANSP code. The model shows that the mixing radius and the number of particles involved in the redistribution decreases with increasing energy. This is consistent with the experimental data presented in Fig. 12. The relative C^{5+} radial density profile is also shown as derived from multichord spectroscopic measurements of the C^{5+} line 5291 Å. The radial distribution of the

brightness has been transformed using Abel inversion to obtain the emissivity of the 5291 Å line. The relative C^{5+} density profile has been calculated by the dividing of the emissivity by the local electron density of the plasma. The dependence of the emissivity on the variation of electron temperature with major radius was assumed to be negligible in the range of the plasma electron temperature 1.5 ± 1.0 keV.

To normalize the model calculations to the experimental data, the emissivity distribution of the reaction $H^+ + C^{5+} = H^o + C^{6+}$ over the major radius was calculated and the results for different energies of H^+ ions are presented in Fig. 15. The vertical axis of the plot is the product of H^+ density, C^{5+} density and plasma transparency $\mu(E,R)$. The values of $N(H^{+})$ and $N(C^{5+})$ are taken from Fig. 14. The passive experimental spectra for the period before the crash (circles) and after the crash (squares) are shown in Fig. 15. Note that the spectrum before the crash consists of the signals coming from the resonance at the plasma center only whereas the signals after the crash come from both the resonance region and the redistributed H^+ ions. The model spectra (solid lines) are the results of integration over the major radius of the emissivity multiplied by the transparency, $\mu(E)$, for the noted H^+ energies. The model and experimental spectra are normalized at one point. To obtain agreement between the model and the experimental data, it was necessary to use the adjustable parameter $E_{crit} = 317$ keV which corresponds with $\tau_{crash} = 50$ μs and a helical electric field $E_e = 1.4$ kV/cm in the model. Here E_{crit} is adjustable critical energy which equal to the energy of the particles having toroidal precession time equal to the crash time. Note that according to [20], particles with $E>E_{crit}$ average the effect of the electric field during the toroidal precession and are less affected by the crash than particles with the energy $E<E_{crit}$. Comparing the experimental and calculated energy spectra shown on Fig. 13b we can conclude that the mixing model is in good agreement with the experimental data when reasonable values of adjustable parameters are assumed.

Our understanding of the mechanism for generation of the H^+ signals observed in the presence of the sawtooth crashes is illustrated well by the data presented in Fig. 16. Here the time history of a TFTR discharge with ICRF-driven H^+ minority ions and with a short D^o neutral beam pulse is shown. The H^+ signal spikes generated by the giant sawtooth crash are seen as well as the signal increase during the NB blip. The H^+ signals due to the crash decrease with increasing H^+ energy in accordance with the model described above. The relative level of H^+ signals in the presence of the NB blip remains approximately constant for all measured energies. Note that on TFTR the NPA observation line does not directly view any of the heating beams injected into the plasma. Therefore the signal cannot be the result of direct charge-exchange of H^+ ions with the D^o atoms of the beam. The origin of this signal is described in detail in [4]. According to this paper, the

heating beams injected into the tokamak plasma change the ionization balance of the carbon ions and lead to an increase of the C^{5+} density in the plasma core because of the increasing probability for electron capture by C^{6+} ions from the beam. It was shown that in JET the injection of the heating beams leads to an increase of the C^{5+} density by a factor of 3 - 4 not only in the vicinity of the beams but all around the torus. The same phenomenon obviously occurs in TFTR. It is important to note that the decrease of the H^+ signal due to the crash with increasing H^+ energy and the complete absence of the signal above an energy 0.855 MeV (see Fig. 16) is evidence that there are no significant change in the C^{5+} population in the plasma core during the sawtooth crash.

V. Stochastic Ripple Diffusion Losses of ICRF-Driven H^+ Ions due to Sawtooth Mixing.

To simulate the H^+ minority confinement in the TFTR post sawtooth crash plasma, we used the ORBIT [23 - 25] guiding center code. In the ORBIT code, particle motion is calculated in toroidal magnetic geometry using a computed equilibrium and ripple magnetic fields. Fig. 14 presents the locations of the stochastic diffusion domains calculated with the ORBIT code (~ 400 particles were followed) for specific energies (0.25 MeV, 0.5 MeV and 0.75 MeV) and for the experimental pitch-angle, $v_{||}/v$ = - 0.048. The orbit code predicts that the ions whose banana tips are located inside these domains are lost in a few milliseconds because of the stochastic ripple diffusion. Outboard of these domains is the region of prompt first orbit loss. It is seen from Fig. 14 that the TFTR ICRF-driven trapped H^+ ions are transported outward after the giant sawtooth crash and reach the stochastic domains. A fraction of the ions can pass through these domains and even reach the prompt loss region.

For more detail analysis of the H^+ confinement time inside the stochastic domains, 5,000 particles with energies of 0.266, 0.322 and 0.4 MeV were followed. The results of this analysis are presented in Fig. 17. Here the light curves are smoothed experimental H^+ signals which occur immediately after the crash (crash occurs at zero time). The solid lines show ORBIT code simulations of the H^+ decay due to the stochastic ripple diffusion losses. The initial radial distributions of the minority ions in the model were chosen to represent the population of H^+ minority ions giving the maximum contribution to the PCX signal (maximum of the emissivity for each measured H^+ energy, Fig. 15). The initial radial location of the H^+ ions is indicated in the legend on Fig. 17. We used a uniform distribution in space and pitch angle so that the bounce point was at a major radius ranging from 3.2 m to 3.3 m with the vertical coordinate Z = 0 - 0.30 m. The results show that the

minority ions of interest are all lost after ~10 - 12 ms and their density evolution may be given roughly by the expression $n(H^+) = n_o(H^+) \exp(-t/\tau_{st})$ where τ_{st} is equal to 3.5 ms, 4.1 ms and 5.5 ms for specified H^+ energies. The confinement time of H^+ ions increases with increasing energy because the signals for ions with higher energies originate from deeper regions if the plasma where the influence of the stochastic ripple diffusion is weaker. It is seen that the ORBIT results are in a good agreement with the experimental data. This result corroborates the model [18] used for sawtooth mixing of fast particles, since an incorrect H^+ post sawtooth distribution in major radius will change the computed decay time and spoil the oberved agreement.

Above we discussed the influence of giant sawteeth ($\Delta T_e/T_e \sim 30\%$) on H^+ ions. Figure 18 shows the time history of a TFTR discharge with smaller periodic sawtooth oscillations ($\Delta T_e/T_e \sim$ 10-15 %). We can see here that there are no changes in either the passive charge exchange H^+ signal or the lost H^+ ion signal. This means that in this case the H^+ mixing radius is much smaller than in the case of the giant sawteeth. If we will assume that the C^{5+} density distribution in this plasma is similar to those shown in Fig. 14, we can conclude that the H^+ mixing radius in this case is less than 30 - 35 cm. Therefore the smaller sawteeth do not lead to sufficient H^+ redistribution to produce noticeable stochastic ripple diffusion losses.

VI. Conclusions

Measurements of ICRF heated H^+ ions in deuterium plasmas in TFTR based on the use of neutral particle analysis in the MeV energy range can provide important information on the energy balance of those ions. It was shown that the diffusion-like losses of H^+ ions during ICRF heating lead to a limitation of the H^+ effective temperature to about 0.15 MeV at P_{ICRF} = 2 MW and to 0.35 MeV at 6 MW as well as to the degradation of the confinement time from ~ 0.3 s (1 MW) to ~ 0.15 s (6 MW). The most probable cause of the H^+ losses is the TAE-like modes excited by the H^+ minority tail at ICRF power exceeding 3 - 4 MW in TFTR.

It was shown also that strong, low frequency MHD events like giant sawtooth crashes ($\Delta T_e/T_e \sim 30\%$) which occur during ICRF heating cause a strong redistribution of H^+ ions outward along the major radius. This redistribution leads to stochastic ripple diffusion loss of H^+ ions. This does not occur in smaller periodic sawtooth oscillations where $\Delta T_e/T_e \sim$ 10-15 %. The observations are consistent with a model for the redistribution of energetic particles developed earlier to explain the results of DT alpha-

particle redistribution due to sawtooth crashes that were observed on TFTR and also with ORBIT code simulations of H^+ stochastic diffusion ripple losses.

Acknowledgments

Work Supported by U. S. DoE Contract No. DE-AC02-76CH03073. Informative discussions with R. Nazikian are greatly appreciated.

References

1. KISLYAKOV, A. I., et al., Fusion Engineering and Design **34-35** (1997) 107.

2. PETROV, M. P., et al., in 1992 International Conference on Plasma Physics (Proc. Con. Innsbruck 1992), Vol. 16C, Part II, European Physical Society, Geneva (1992) 1031.

3. KHUDOLEEV, A.V., et. al., in Radiofrequency Heating and Current Drive of Fusion Devices (Proc. Top. Conf., Brussels, 1992), Vol. 16E (1992) 117.

4. KOROTKOV, A.A., et.al., Nucl. Fusion **37** (1997) 35.

5. AFANASSIEV, V. I., et al., Proceedings of the 22nd European Physical Society Conference on Controlled Fusion and Plasma Physics, edited by B.E. Keen, P.E. Stott., and J. Winter (The European Physical Society, Bournemouth, UK, 1995), Vol. 19C, P. II-057.

6. FISHER, R. K. et.al., Phys. Rev. Lett. **75** (1995) 846.

7. MEDLEY, S. S., et al., Rev. Sci. Instrum. **67** (1996) 3122.

8. BARNETT, C. F. (Ed.), Atomic Data for Fusion, Vol. 1, Rep. ORNL-6086/VI, Oak Ridge Natl. Lab., TN (1990); ibid., Vol. 5, Rep. ORNL-6090.

9. McCHESNEY, J. M., et al., Rev. Sci. Instrum. **66** (1995) 348.

10. TCHERNYSHEV, F. V., private communication.

11. WONG, K. L., et. al., Phys. Plasmas **4** (1997) 393.

12 KOLESNICHENKO, Ya. I., et al., Nucl. Fusion **36** (1996) 159.

13. MARCUS, F.B., et al., Nucl. Fusion **34** (1994) 687.

14. DUONG, H. H. and HEIDBRINK, W. W., Nucl. Fusion **33** (1993) 211.

15. PETROV, M. P., et al., Nucl. Fusion **35** (1995)1437.

16. PETROV, M. P., et al., in Proceedings of 16th IAEA Fusion Energy Conference, Montreal, Canada, October 1996. “Fusion Energy 1996”, IAEA Vienna 1997, Vol.1 p 261.

17. MEDLEY, S. S., et al., to appear in Nucl. Fusion (June, 1998).

18. DARROW, D. S., et.al., Nucl. Fusion **37** (1997) 939.

19. BOIVIN, R. L., et al., Nucl. Fusion **33** (1993) 449.

20. GORELENKOV, N. N., et al., Nucl. Fusion **37** (1997) 1053.

21. BUDNY, R. V. et al., Nucl. Fusion **35** (1995) 1497.

22. KADOMTSEV, B. B., Soviet Plasma Phys. **1** (1976) 389.

23. WHITE, R. B. and CHANCE, M. S., Phys. Fluids **27** (1984) 2455.

24. WHITE, R. B., Phys. Fluids B **2** (1990) 845.

25. WHITE, R. B., et al., Phys. Plasmas **3** (1996) 3043.

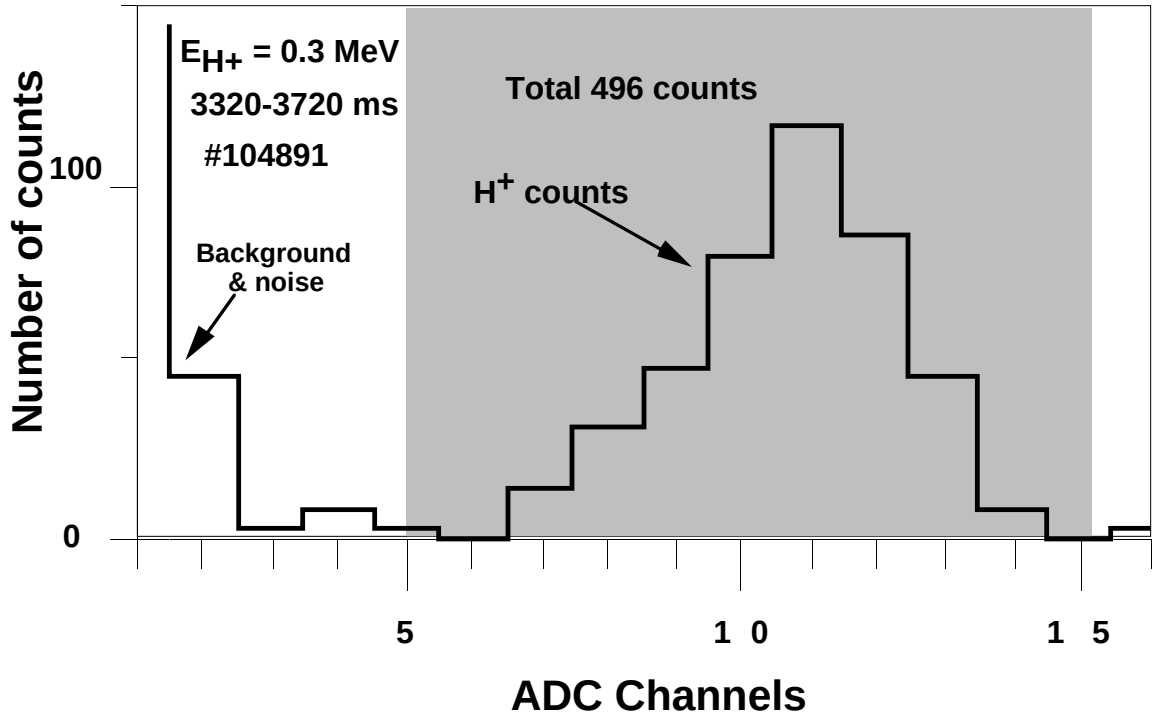

Fig. 1 Typical pulse height distribution in the PCX pulse counting mode during ICRF minority heating. In all 8 channels of the NPA, the H^+ signal is well separated from the neutron-induced background noise.

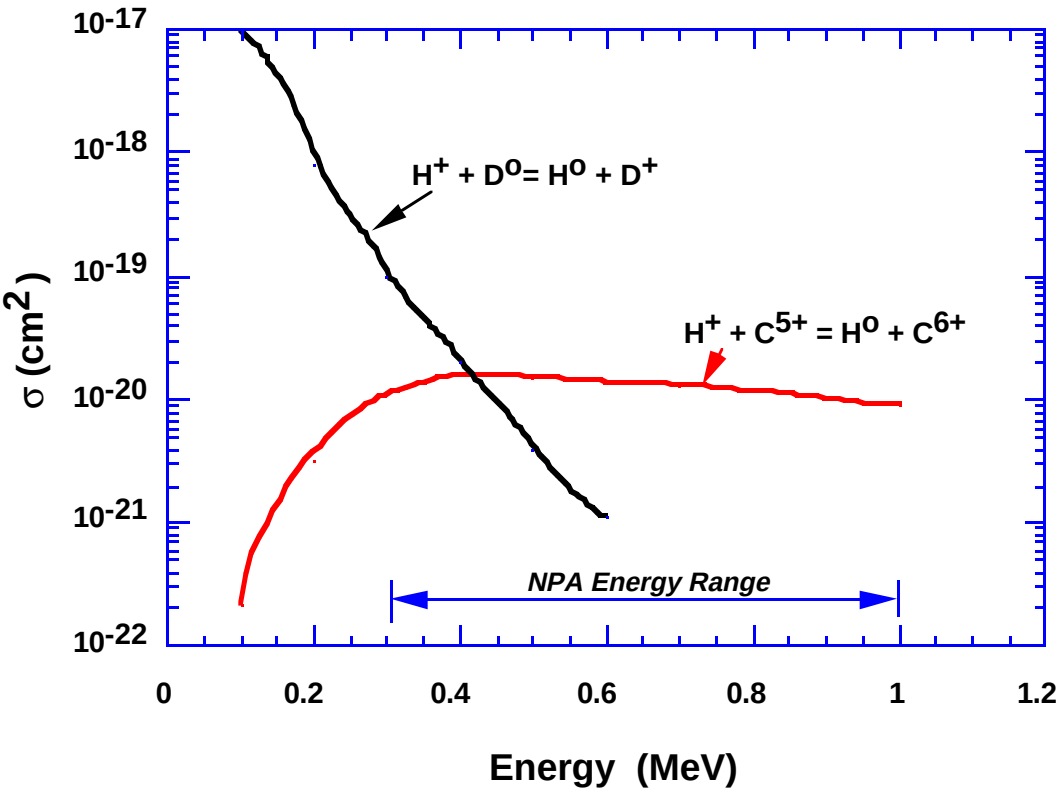

Fig. 2 Cross sections for charge-exchange by protons with D^o atoms[8] and with C^{5+} impurity ions[4].

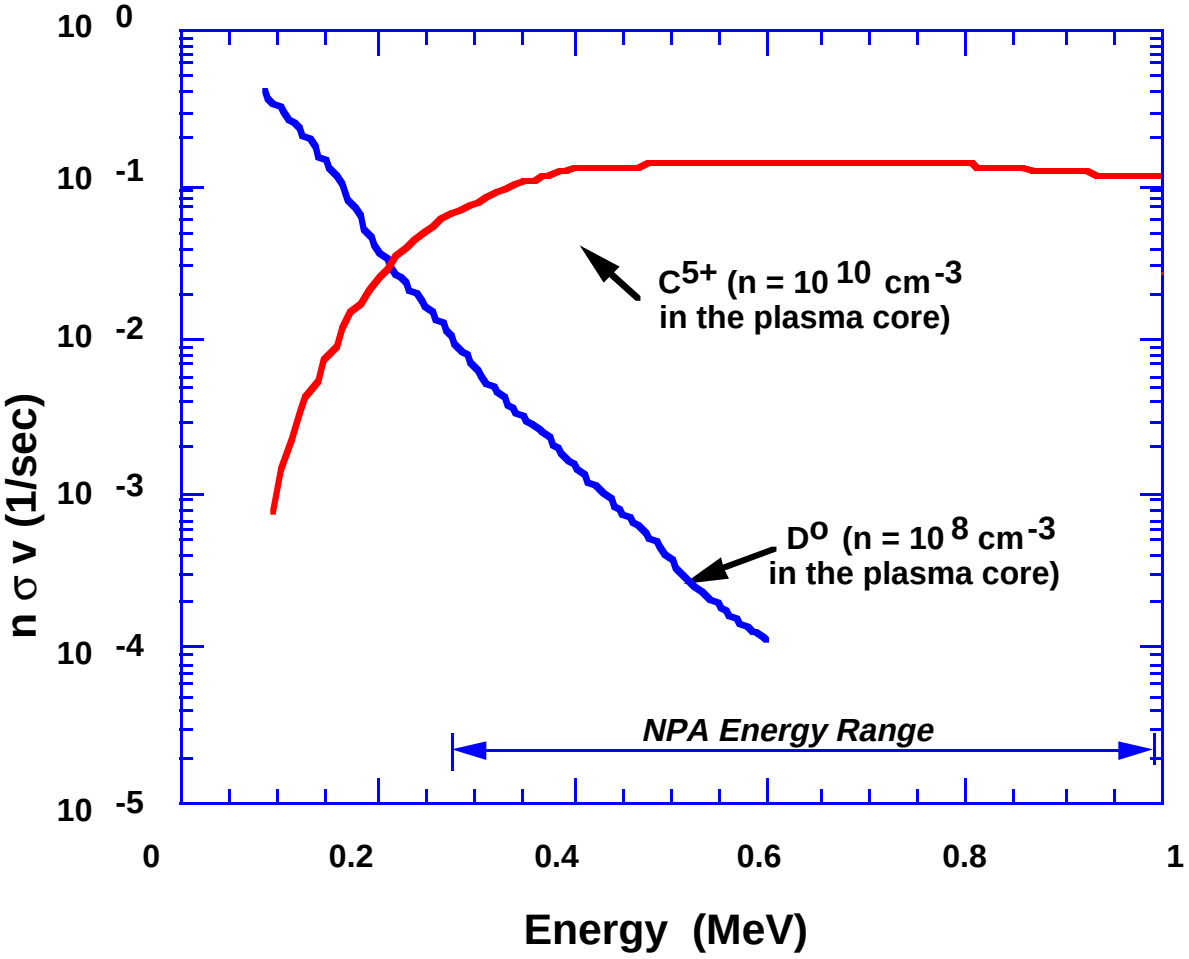

Fig. 3 Charge-exchange rates of H^+ ions with C^{5+} ($n = 10^{10}$ cm^{-3} in the TFTR plasma core) and with D^o ($n = 10^8$ cm^{-3} in the plasma core). The C^{5+} cross section dominates at the higher H^+ energies of interest in the NPA measurements.

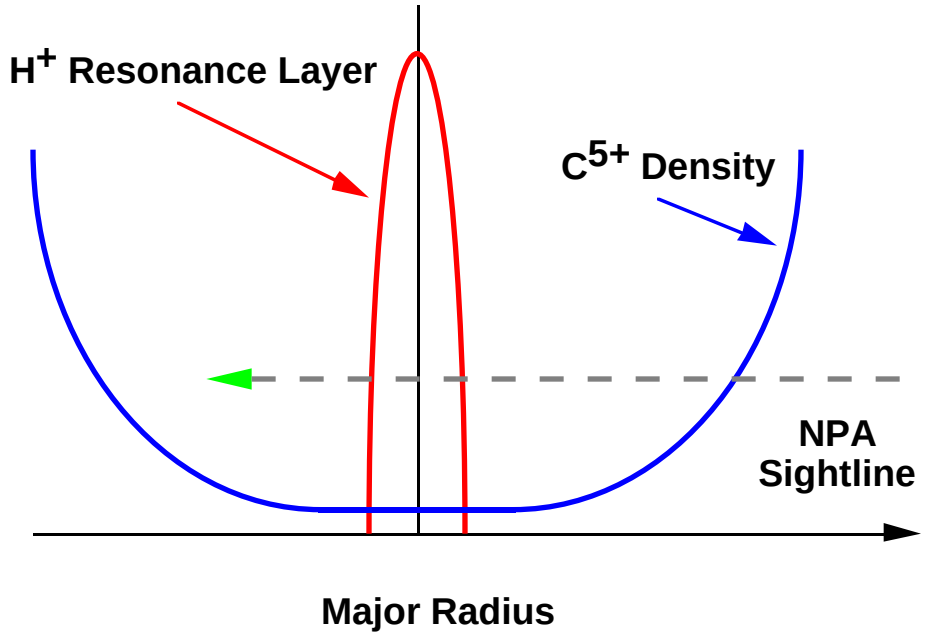

Fig. 4 Schematic illustrating passive H^+ diagnostic integration over the NPA sightline. Note that the H^+ energetic ion distribution to be measured is core-localized while the C^{5+} charge exchange donor is edge-weighted.

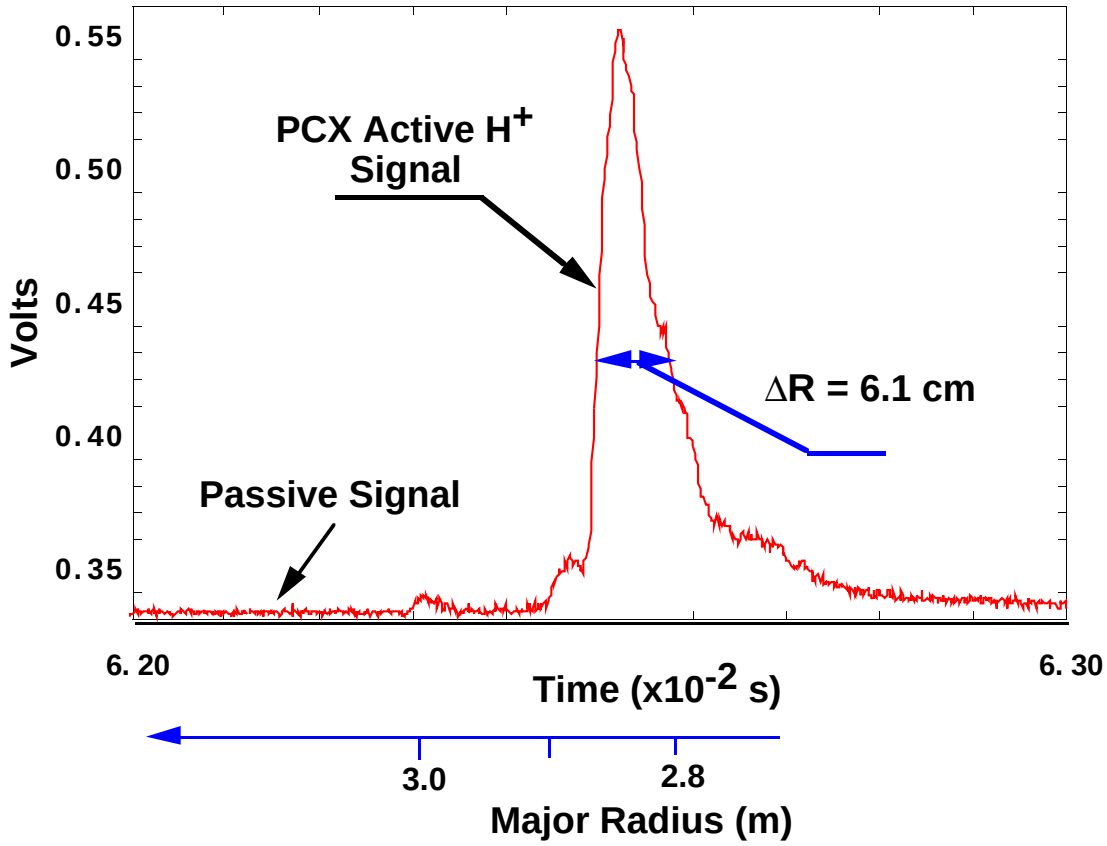

Fig. 5 The radial position and shape of the H^+(E = 0.72 MeV) resonance measured by the PCX active diagnostic for fundamental H^+ ICRF heating in a TFTR deuterium plasma. Measurements from a look-down photodiode array are used to convert the pellet-induced active PCX signal from the time domain to radial position in the plasma.

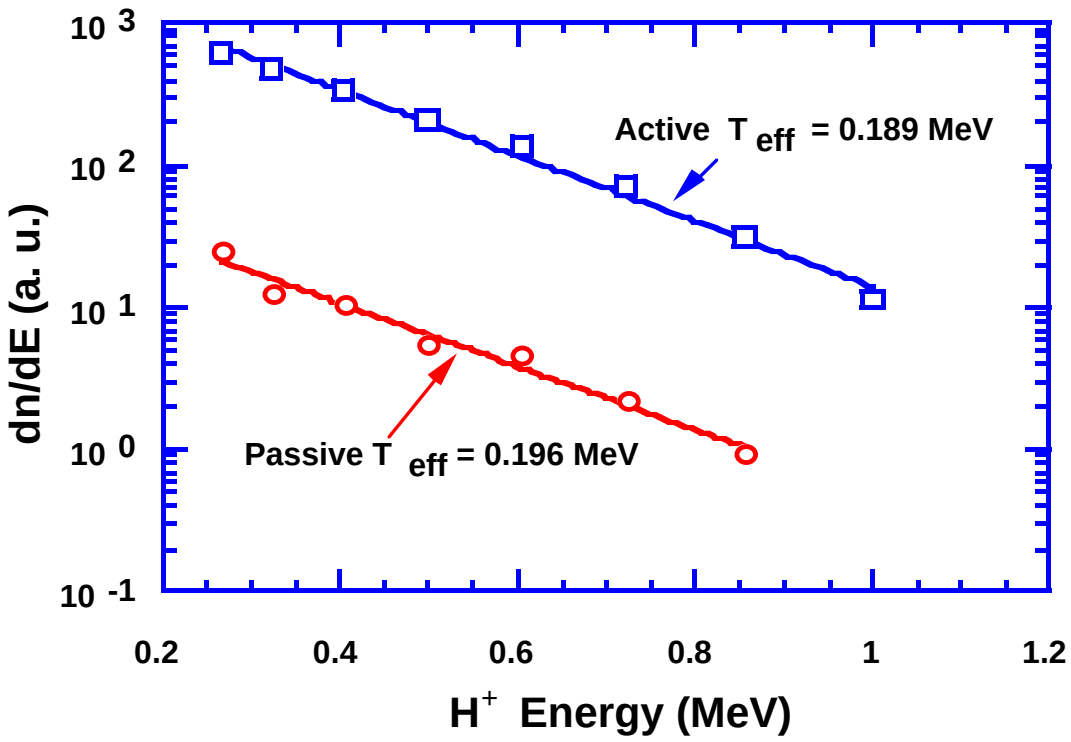

Fig. 6 Active and passive energy spectra of H^+ ICRF driven minority ions in a TFTR deuterium plasma are in close agreement. Both discharges were obtained with on-axis heating at P_{ICRF} = 2.1 MW, F = 43 MHz, Ne(0) = 5.10^{13} cm^{-3}.

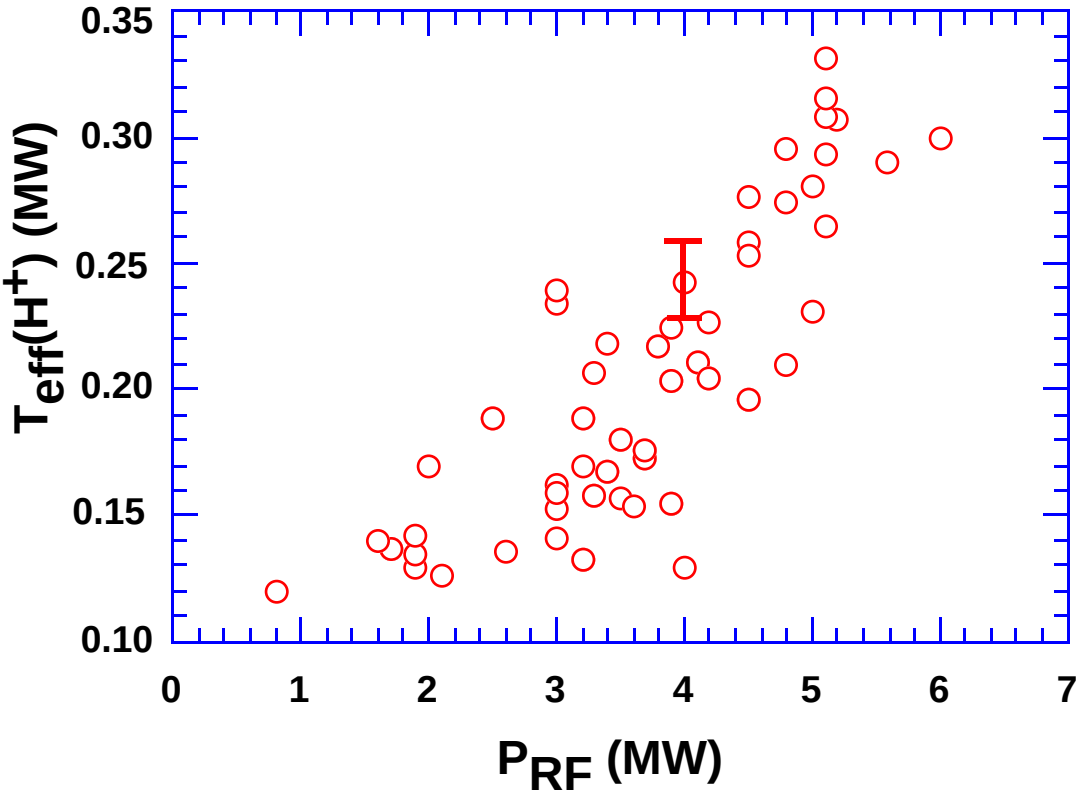

Fig. 7 H^+ effective temperatures versus ICRF power for on-axis ICRF-heated deuterium plasmas in TFTR. The error in the T_{eff} measurements was typically 10 - 15%.

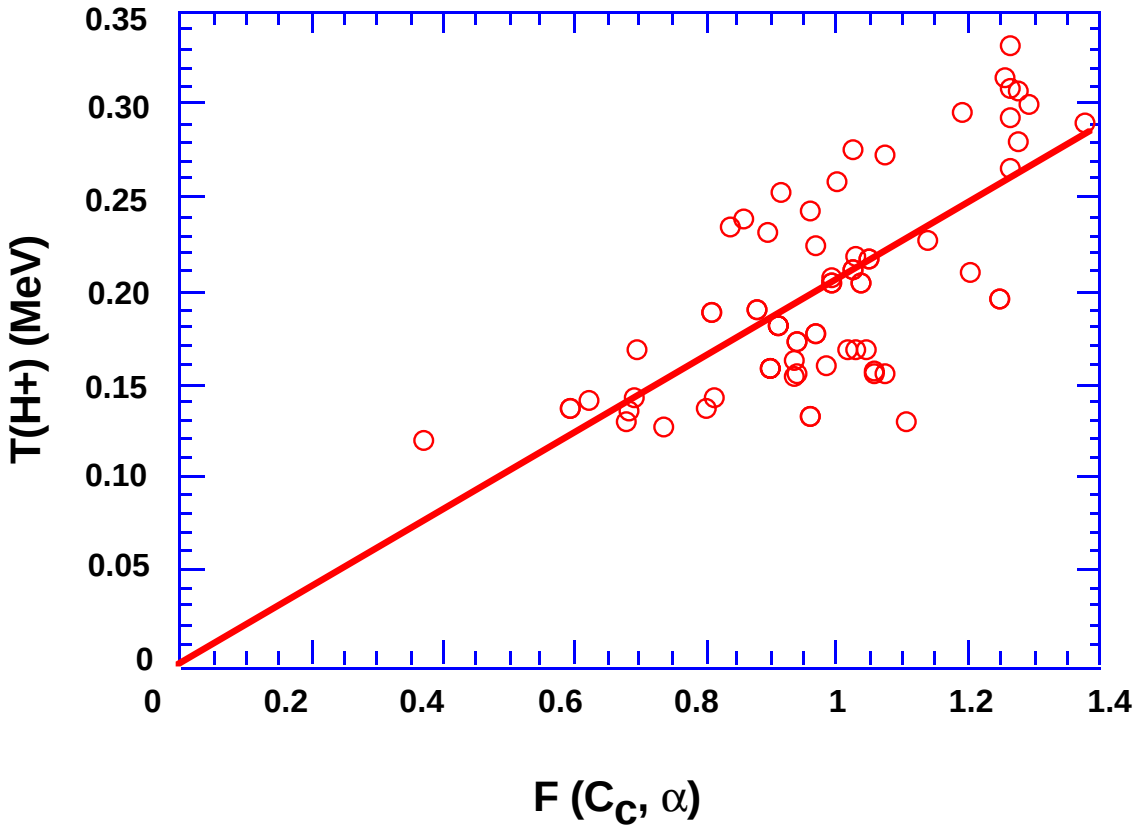

Fig. 8 Plot of H^+ effective temperature data versus the scaling function, $F(C_C, \alpha)$. The solid line is a linear fit for $C_C = 0.018 \pm 0.001$ and $\alpha = N_H/N_e = 0.05$.

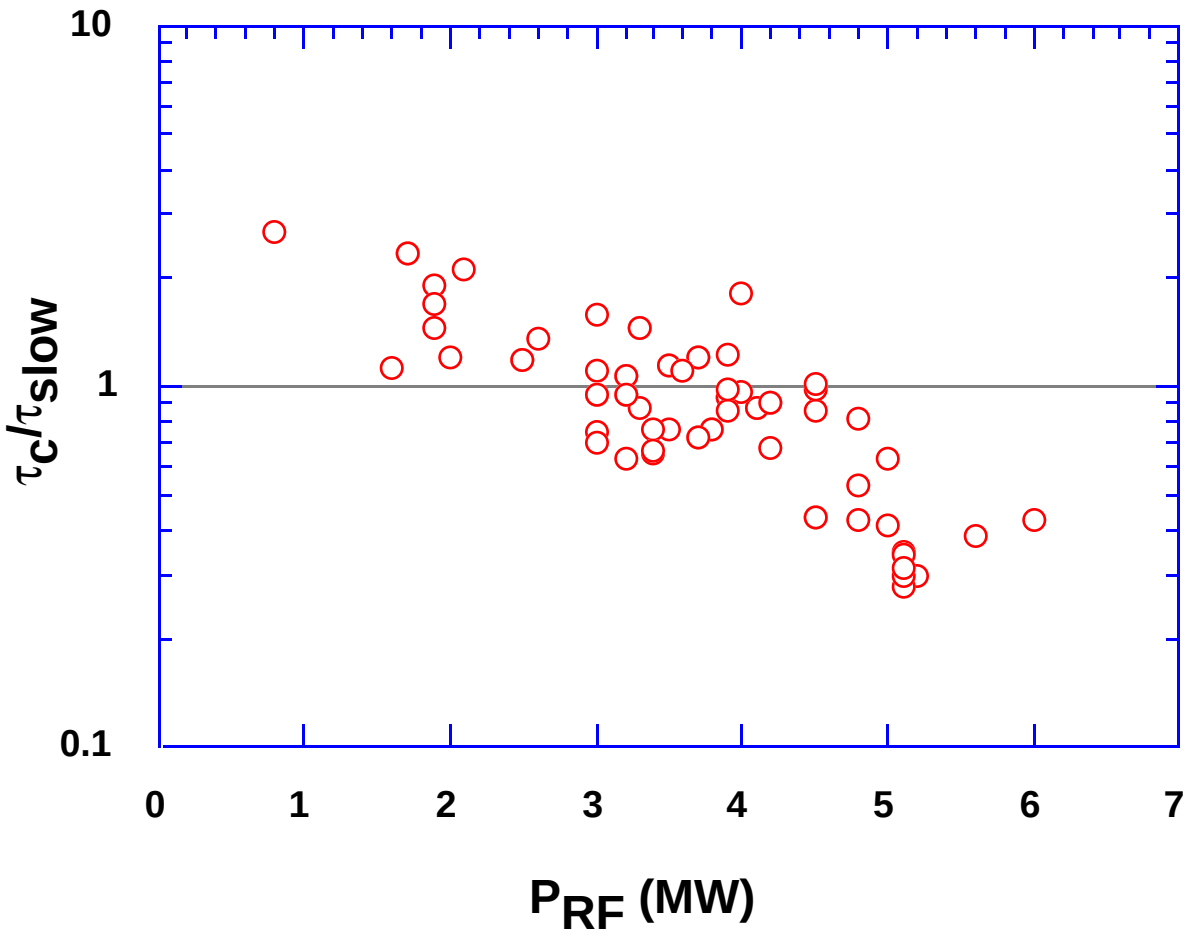

Fig. 9 The ratio of the confinement time to the slowing down time, τ_c/τ_{slow}, decreases with increasing ICRF power for H^+ the ICRF driven minority ions in TFTR ($\alpha = N_H/N_e = 0.05$).

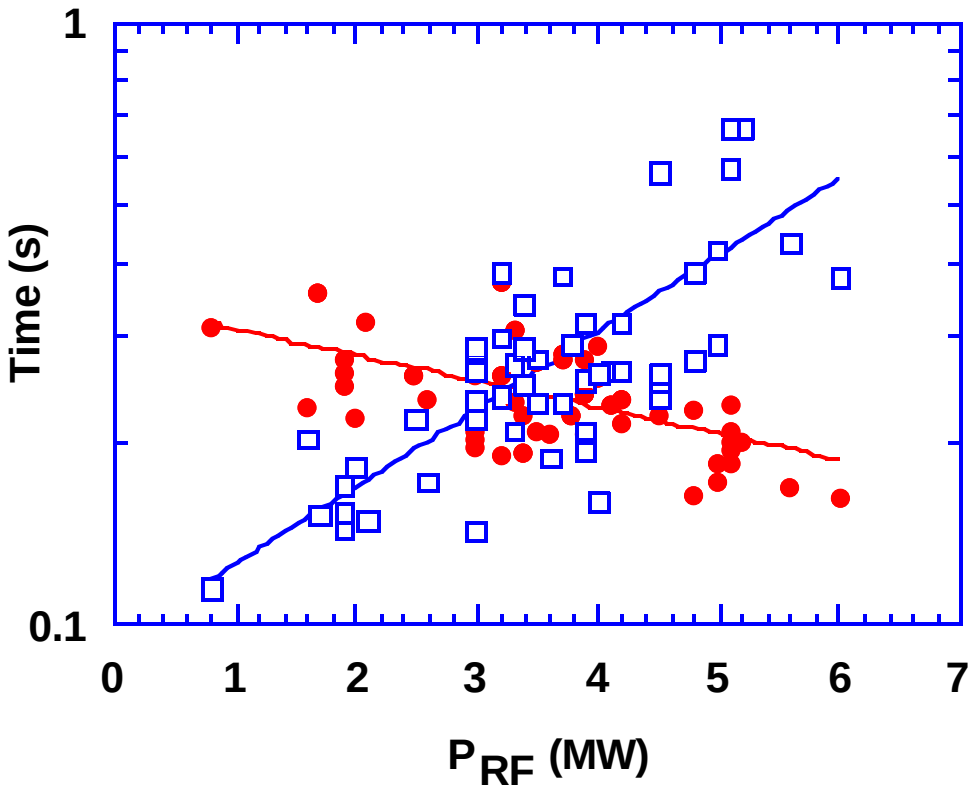

Fig. 10 The confinement time, τ_c (circles), decreases and the slowing down time, τ_{slow} (squares), increases with increasing ICRF power for H^+ ICRF-driven ions in TFTR. The lines are exponential fits.

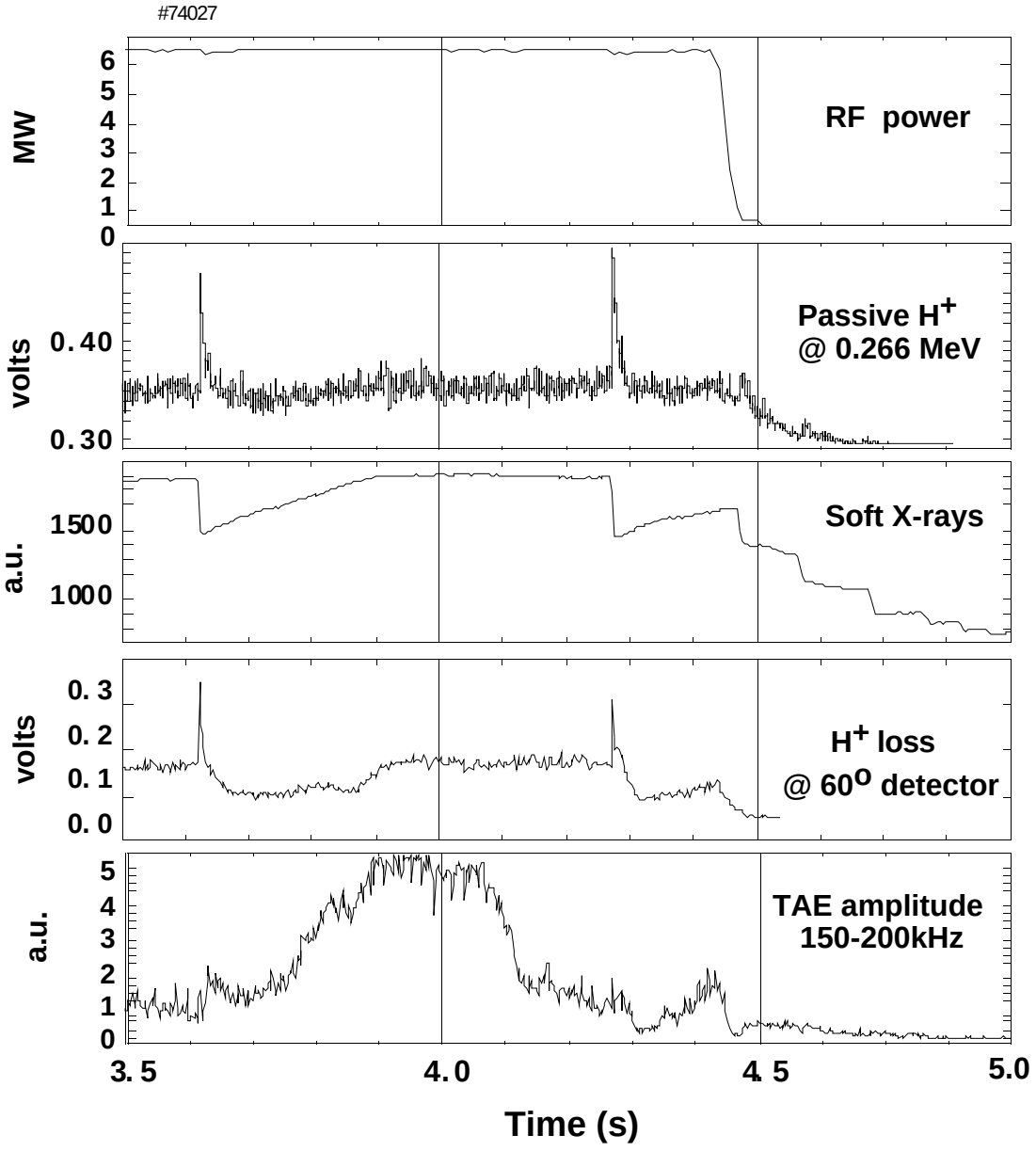

Fig. 11 Shown is the time history of a discharge with ICRF-driven H^+ minority heating including: ICRF power, passive H^+ signal (0.266 MeV), soft X-ray signal showing two giant sawtooth crashes, tail loss rate at the 60^o lost alpha detector and a Mirnov signal exhibiting the ICRF tail ion driven TAE.

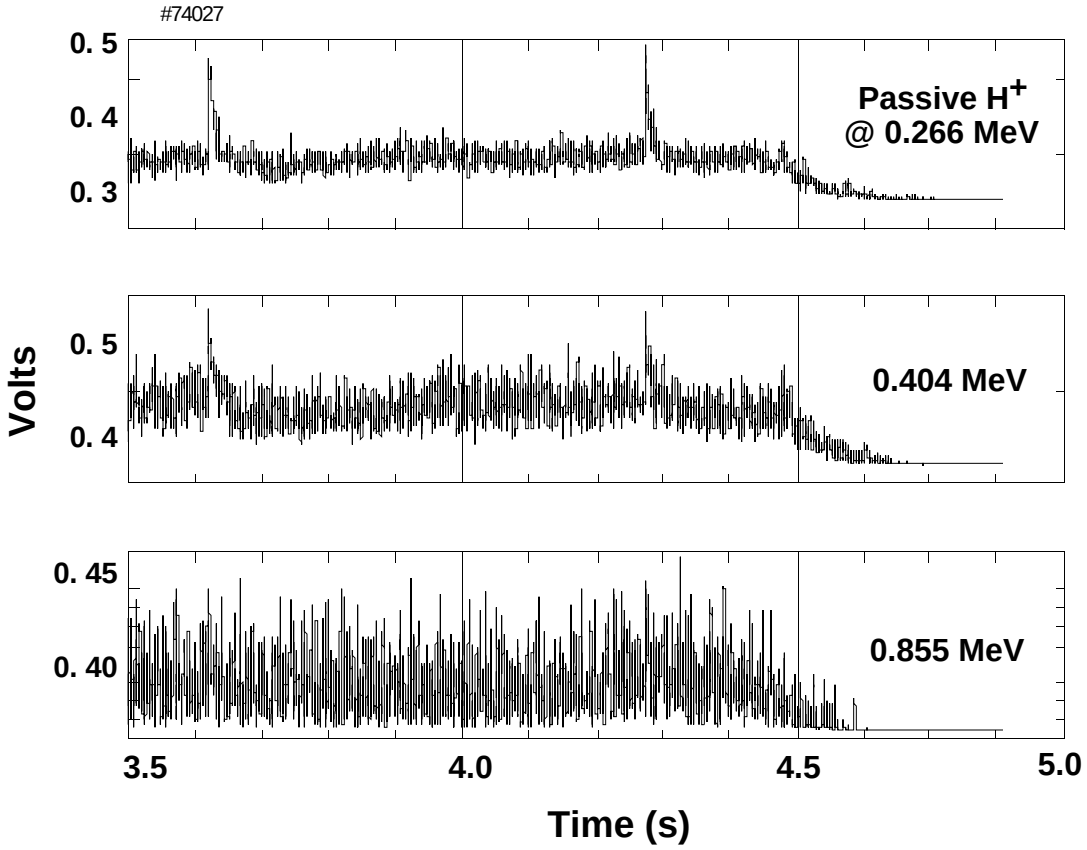

Fig. 12 Passive signals for ICRF driven H^+ minority ions of different energies in the presence of two giant sawtooth crashes (the same discharge as Fig. 11).

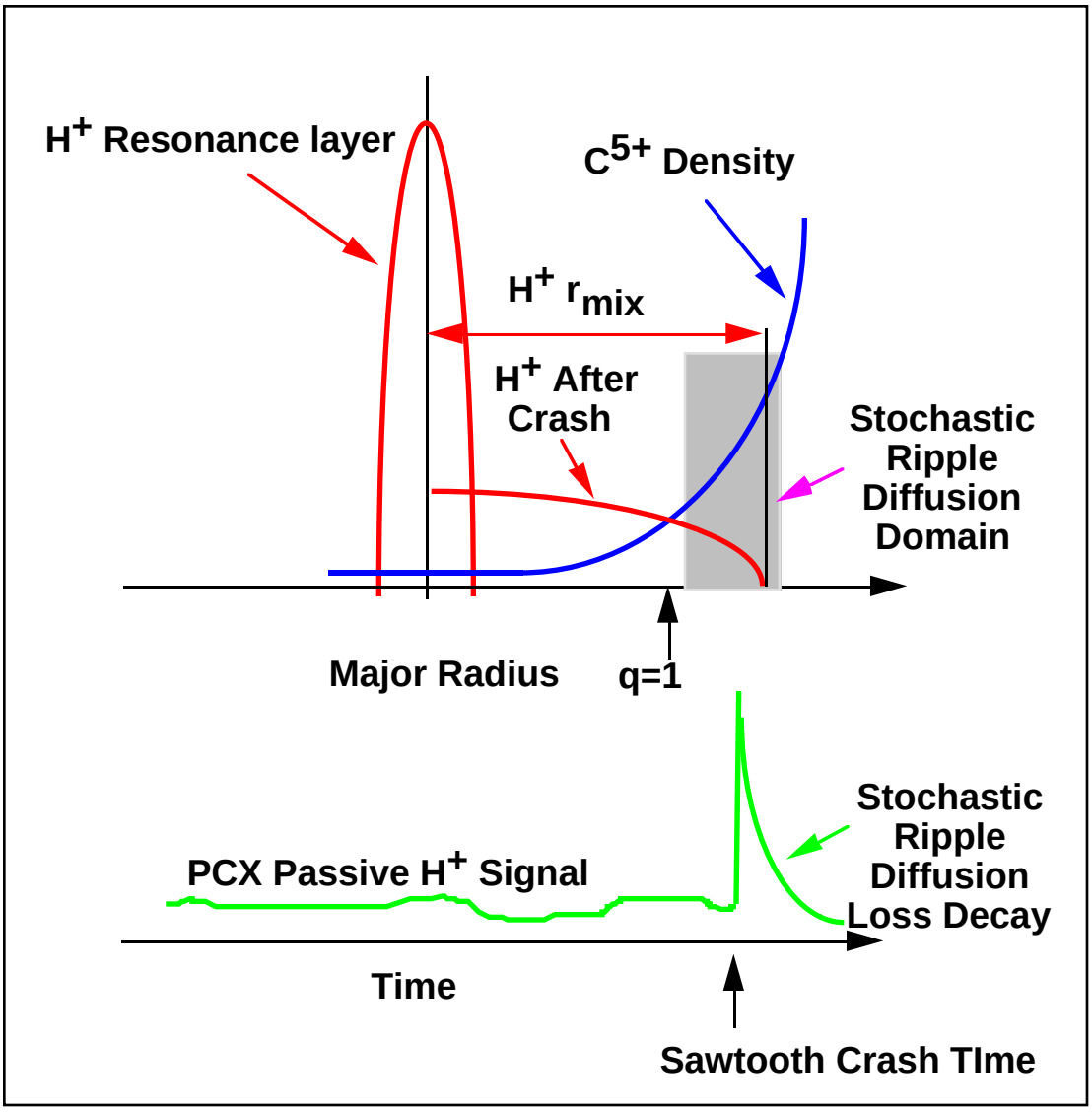

Fig. 13 Schematic illustrating the origin of the H^+ passive charge exchange signal generated by H^+ sawtooth mixing.

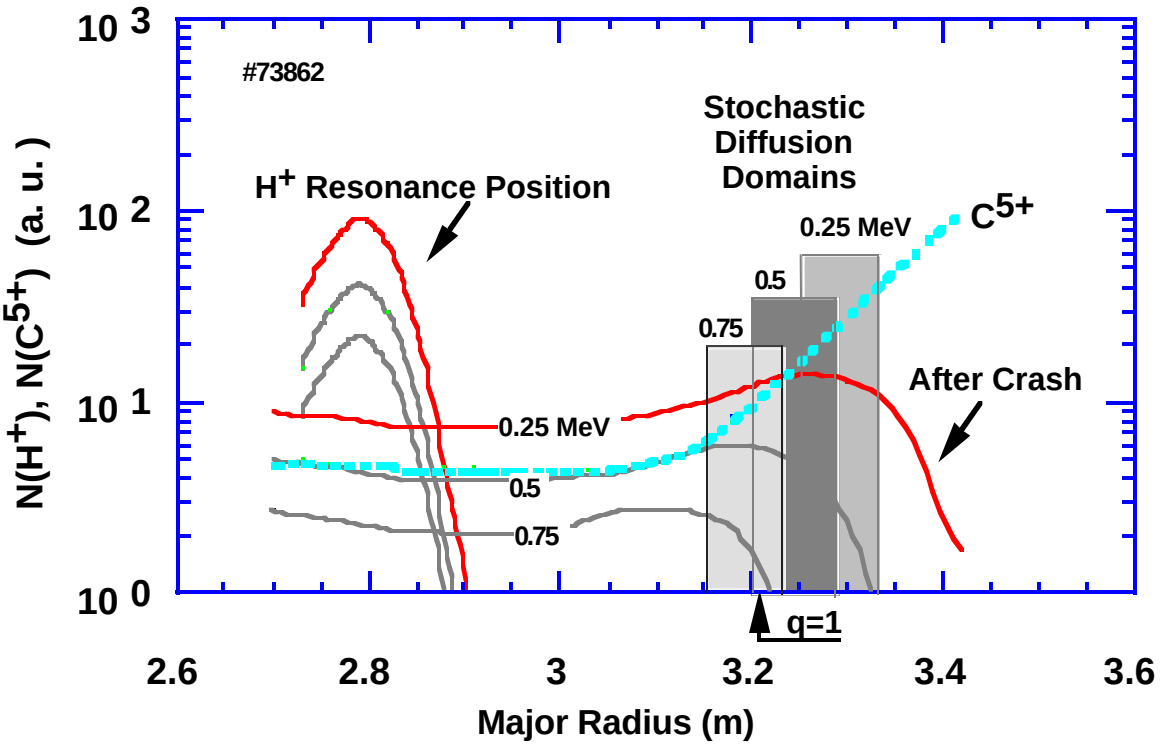

Fig. 14 Modeling results are shown for the ICRF-driven H^+ ion sawtooth mixing. Three H^+ energies (0.25, 0.50 and 0.75 MeV) are presented before and after the sawtooth crash. Adjustable parameters used in the modeling were E_{cri} = 317 keV, E_e = 1.4 kV/cm and $\tau_{pr} = \tau_{cr}$ = 50 μs. The radial locations of the stochastic ripple domains for the noted H^+ energies are shown by the hatched regions. The dotted line is the C^{5+} radial density distribution.

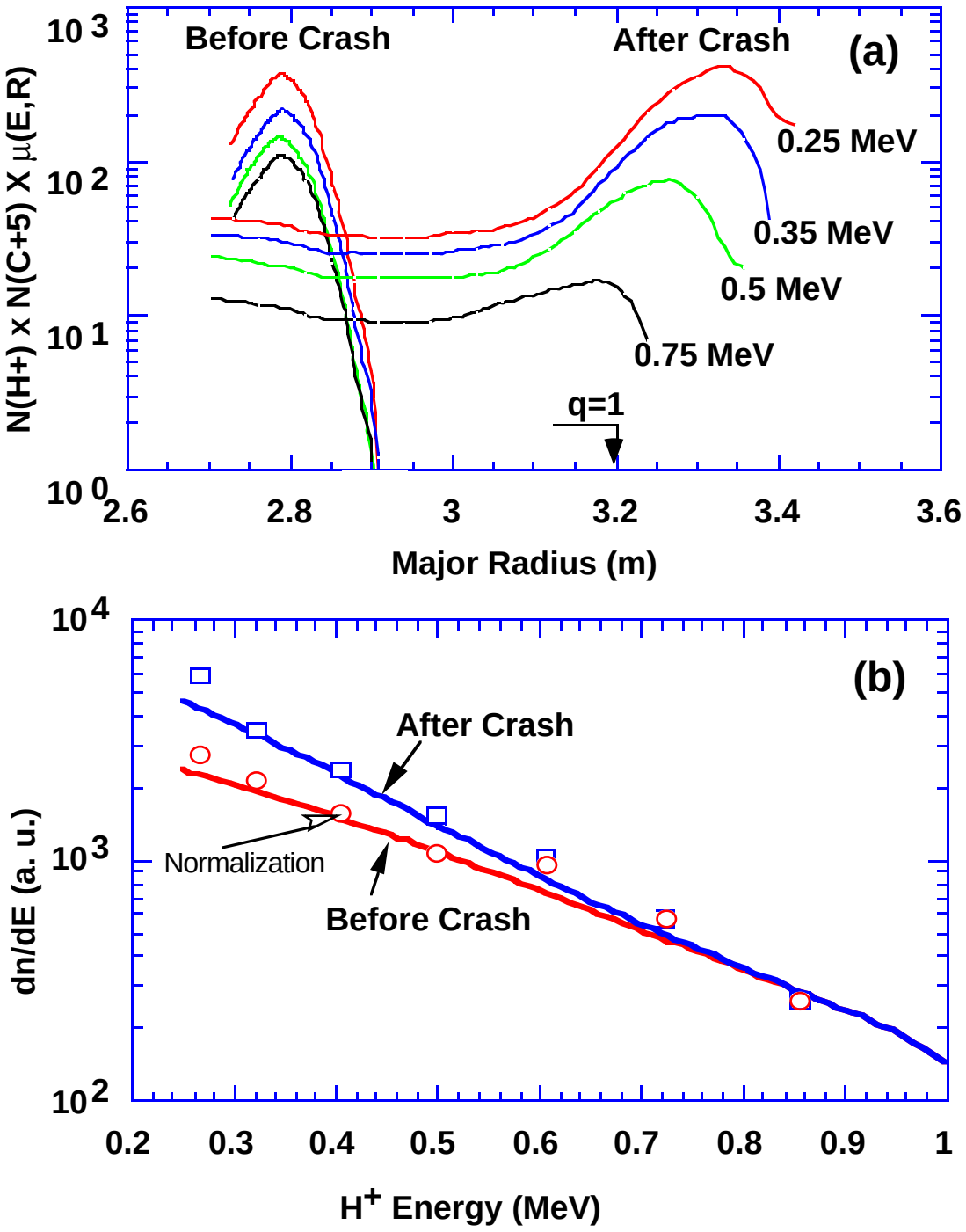

Fig. 15 Shown are the emissivity of the $H^+ + C^{5+}$ reaction versus major radius (a) and the energy spectra before and after the crash integrated over the observation line (major radius) on the basis of the presented emissivity (b). Solid lines are model results and data points are passive experimental spectra before and after the crash.

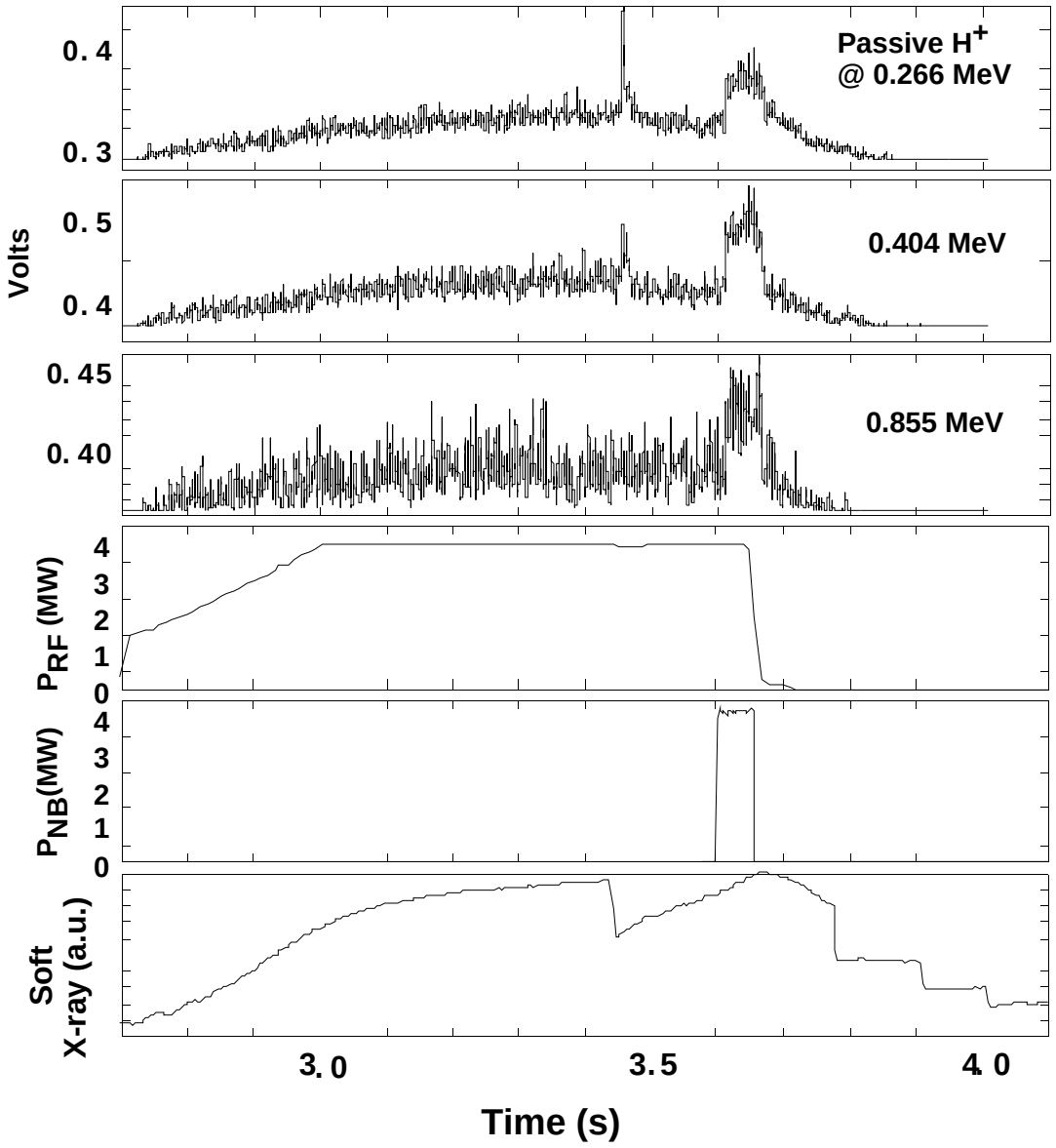

Fig. 16 The time history of a discharge with ICRF-driven H^+ minority ions and a D^o neutral beam blip is shown, including passive H^+ signals (0.266, 0.404, 0.855 MeV), ICRF power, NB power, and a soft X-ray signal indicating two giant sawtooth crashes.

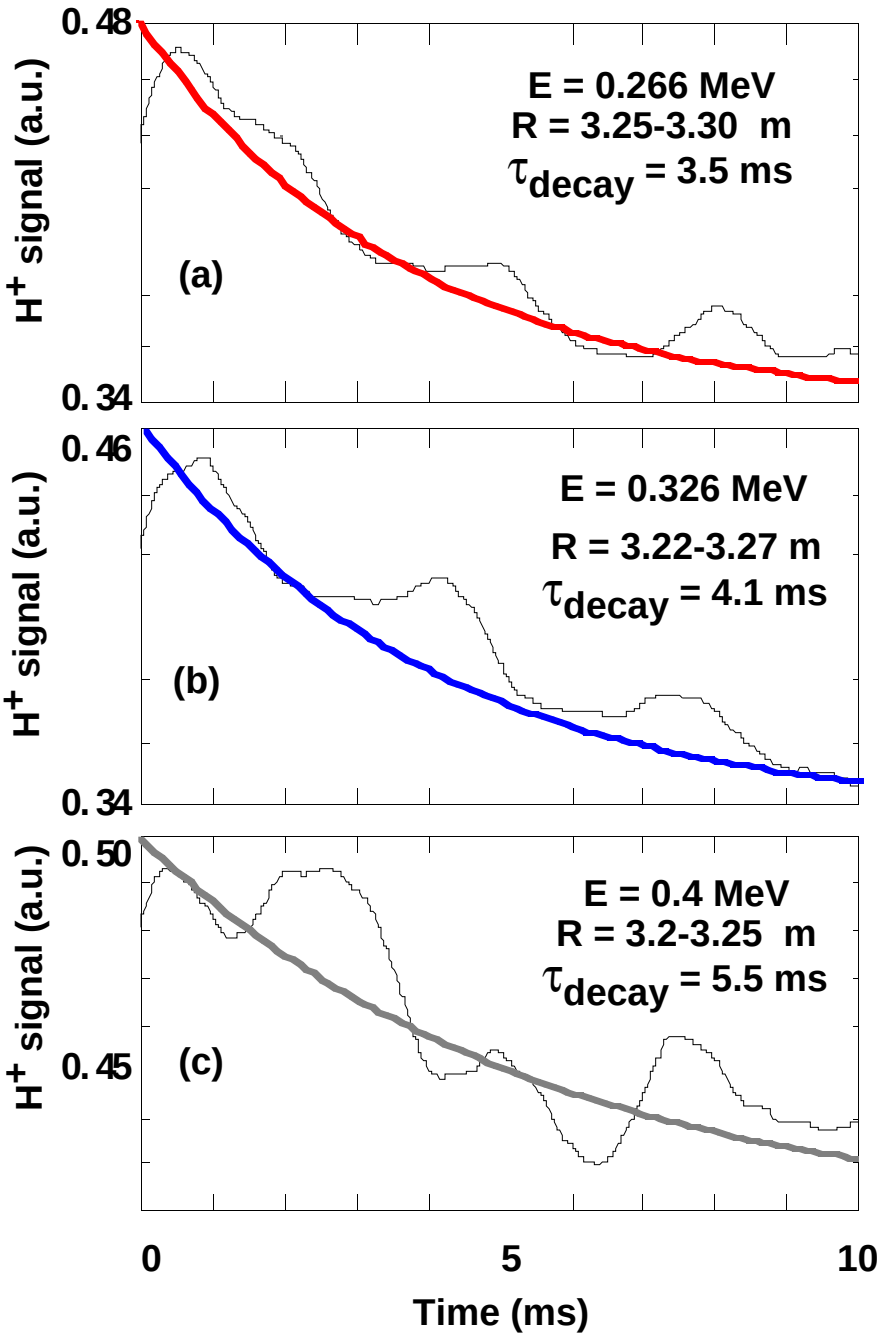

Fig. 17 The decay of the experimental H^+ signal after the giant sawtooth crash and the ORBIT code simulations of this decay, τ_{decay}, due to stochastic ripple diffusion losses are shown for selected H^+ energies.

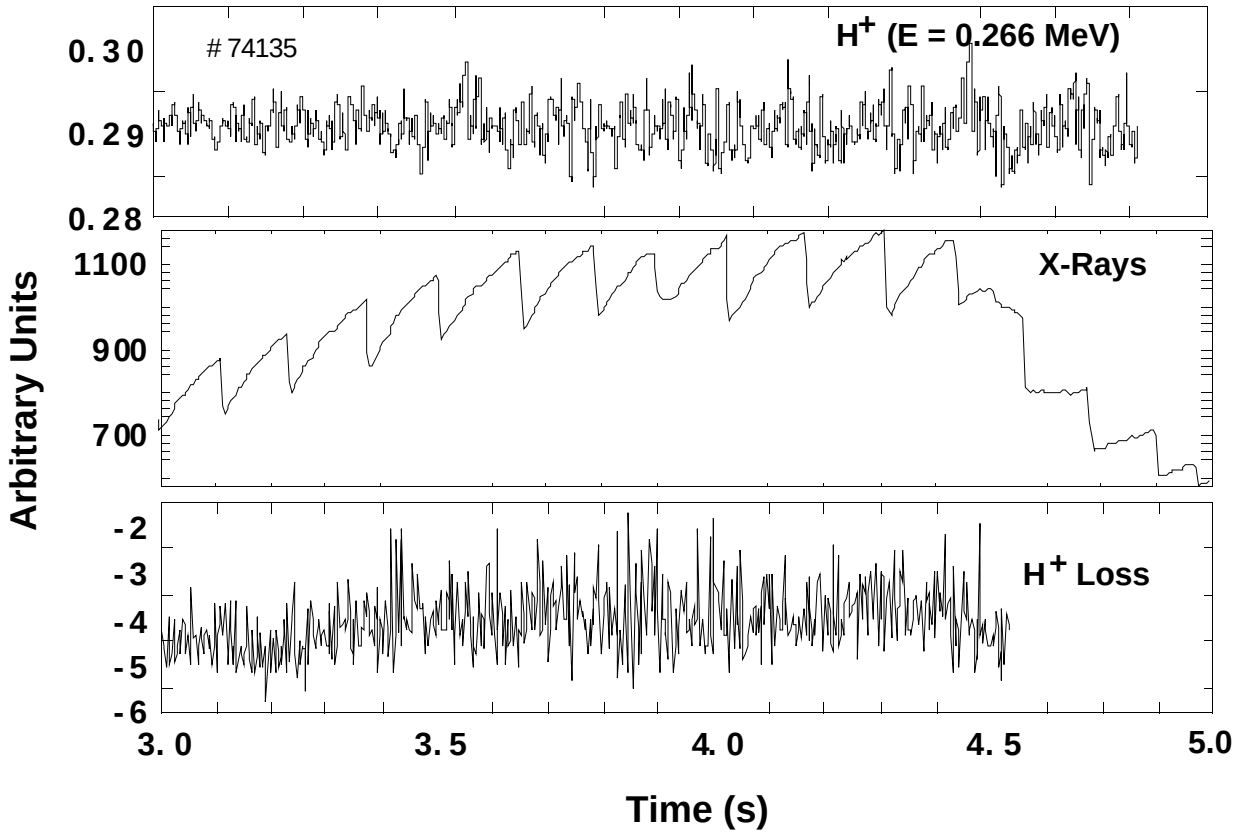

Fig. 18 Shown is the time history of a discharge with ICRF driven H^+ minority (P_{ICRF} = 2.5 MW) including: passive H^+ signal (0.266 MeV), soft X-ray signal (indicating sawteeth oscillations) and H^+ tail loss rate for the 60^o alpha detector. No H^+ redistribution or ion loss is observed for small amplitude sawtooth activity.